JOURNAL OF GEOPHYSICAL RESEARCH, VOL. 104, NO. C6, PAGES 13,251–13,267, JUNE 15, 1999

Three-dimensional isoneutral potential vorticity structure in the Indian Ocean

Mary C. McCarthy and Lynne D. Talley

Scripps Institution of Oceanography, University of California, San Diego, La Jolla

Abstract. The three-dimensional isoneutral potential vorticity structure of the Indian Ocean is examined using World Ocean Circulation Experiment and National Oceanic and Atmospheric Administration conductivity-temperature-depth data and historical bottle data. The distribution of the potential vorticity is set by the Indian Ocean's source waters and their circulation inside the basin. The lower thermocline has a high potential vorticity signal extending westward from northwest of Australia and a low signal from the Subantarctic Mode Water in the south. The Antarctic Intermediate Water inflow creates patches of high potential vorticity at intermediate depths in the southern Indian Ocean, below which the field becomes dominated by planetary vorticity, indicating a weaker meridional circulation and weaker potential vorticity sources. Wind-driven gyre depths have lower potential vorticity gradients primarily due to same-source waters. Homogenization and western shadow zones are not observed. The β-effect dominates the effect of the Somali Current and the Red Sea Water on the potential vorticity distribution. Isopleths tilt strongly away from latitude lines in the deep and abyssal waters as the Circumpolar Deep Water fills the basins in deep western boundary currents, indicating a strong meridional circulation north of the Antarctic Circumpolar Current. The lower-gradient intermediate layer surrounded vertically by layers with higher meridional potential vorticity gradients in the subtropical Indian Ocean suggests that Rossby waves will travel $\sim$1.3 times faster than standard theory predicts. To the south, several pools of homogenized potential vorticity appear in the upper 2000 m of the Southern Ocean where gyres previously have been identified. South of Australia the abyssal potential vorticity structure is set by a combination of the Antarctic Circumpolar Current and the bathymetry.

1. Introduction and Background

Potential vorticity plays an important role in large-scale oceanography, acting both passively as a tracer and dynamically to direct the flow. The potential vorticity distribution reflects features of the large-scale circulation and provides insight into the dynamics which govern it. Potential vorticity is the natural dynamic variable for large-scale circulation and planetary waves, and the conservation of potential vorticity forms the theoretical basis for the circulation as well as for planetary wave propagation.

Theoretical and observational studies of the potential vorticity field have concentrated on the thermocline and the upper wind-driven layers of the ocean. The assumption of Sverdrup dynamics leads to a β-dominated potential vorticity field, which in turn implies that the potential vorticity isopleths follow latitude circles. Several theories explain the mechanisms by which the potential vorticity can be altered from the background β assumption while maintaining the Sverdrup constraint on the vertically averaged flow. In a series of three papers, *Rhines and Young* [1982a, b] and *Young and Rhines* [1982] showed that potential vorticity becomes homogenized inside a gyre's closed streamlines through eddy mixing at thermocline depths that are not directly subject to Ekman layer convergence/divergence. Subtropical gyres shift poleward with depth, and the flow is very weak in regions where potential vorticity isopleths intersect the eastern boundary.

Luyten et al. [1983] considered layers that outcrop and are subsequently subducted, arguing that ventilation sets potential vorticity along characteristics that originate in the outcropping regions. Potential vorticity is then conserved as the subducted water parcel travels around the gyre. Unventilated regions, or shadow zones, exist in this model where streamlines do not intersect the outcrop region.

These theories complement each other: The former does not treat the ventilated layer, while the latter ignores eddies and other transient instabilities. The theories were refined as *Pedlosky and Young* [1983] combined

Paper number 1999JC900028.
0148-0227/99/1999JC900028$09.00

them to show their nonlinear interaction and the flow that results. The basic result is homogenization within the western shadow zone, β structure (no flow) in the eastern shadow zone, and elsewhere potential vorticity set at layer outcrops. Both circulation schemes are reduced in intensity since the Sverdrup transport is divided between them.

Observations and models of the potential vorticity have found many of the features predicted by the above theories [*Holland et al.*, 1984; *Talley*, 1985] and have elucidated other potential vorticity patterns. Looking at potential vorticity on isopycnals to ~2000 m, *McDowell et al.* [1982] considered the North Atlantic, while *Keffer* [1985] examined the world's oceans. These observations showed potential vorticity set in ventilated regions, homogenization in nonventilated regions, and poleward gyre recession with depth. *You and McDougall* [1990] found homogenized neutral surface potential vorticity in the North and South Atlantic wind-driven gyres. *Talley*'s [1988] investigation of the full water column potential vorticity in the North Pacific confirmed previous observations. Her analysis also unearthed a correspondence between areas of Ekman upwelling (tropics, eastern boundary of subtropical gyre, and subpolar gyre) and high potential vorticity. Several studies have used characteristic low potential vorticity to trace the Subtropical and Subpolar Mode Water masses [*McDowell et al.*, 1982; *Talley and McCartney*, 1982; *Keffer*, 1985; *Dewar*, 1986; *Talley*, 1988].

More recent studies have expanded the analysis of potential vorticity to deep and abyssal waters, considering the effects of thermohaline circulation. *O'Dwyer and Williams* [1997] examined the deep and abyssal waters in all of the oceans, finding that potential vorticity often deviates significantly from the β-domination expected from abyssal flow. At middepths, they found patterns to be β-dominated, as observed in the North Pacific [*Talley*, 1988]. However, in the deep and abyssal water, the South Pacific and South Atlantic have inclined (NW-SE) isopleths, while homogenized potential vorticity is found in the North Pacific and North Atlantic. Both patterns suggest relatively vigorous meridional circulation. In the Indian Ocean, *O'Dwyer and Williams* [1997] found that all abyssal levels examined have primarily a zonal potential vorticity distribution except for a slight inclination of isopleths in the bottom water. Any deviations from β were within the error limits of their analysis.

With new observations of Rossby wave propagation revealing phase speeds up to 2 times greater than predicted by standard theory [*Chelton and Schlax*, 1996], recent papers have discussed the theoretical implications of the potential vorticity field through which the waves travel. *Killworth et al.* [1997] and *Dewar* [1998] showed that including a baroclinic mean flow in the analysis gives phase speeds like those observed. In the same vein, *de Szoeke and Chelton* [1999] showed that a three-layer model with a homogenized second layer between higher-gradient first and third layers gives the appropriate shear to account for the observed Rossby wave speed increase.

This study seeks to examine the Indian Ocean's thermocline to abyssal potential vorticity structure, which previous studies have found to be mostly β-dominated. Several high-quality data sets recently have become available, and a more detailed analysis is now possible. The Indian Ocean adds unique features to the study of potential vorticity with its complicated bathymetry, prominent link to the Southern Ocean, and reversing monsoonal currents. Several new studies have carefully examined aspects of the Indian circulation [*Fine et al.*, 1988; *Park et al.*, 1993; *Toole and Warren*, 1993; *Mantyla and Reid*, 1995; *Park and Gamberoni*, 1995; *Hufford et al.*, 1997; *McCarthy et al.*, 1997; *Talley and Baringer*, 1997; *Robbins and Toole*, 1997], providing a helpful background for understanding the observed potential vorticity patterns. Thermocline water masses have been carefully defined [*You and Tomczak*, 1993; *You*, 1996], and they may have unique potential vorticity signals. From TOPEX/POSEIDON data, *Stammer* [1997] found high eddy variability at ~15°S in the Indian Ocean that may be related to changes in the potential vorticity gradient shown below. The active wind-driven currents in the Indian Ocean overlie a strong abyssal circulation, allowing the possibility of comparison between the relative effects of each on potential vorticity. The potential vorticity is mapped on several neutral surfaces to provide a steady state picture of the potential vorticity as well as to develop a better understanding of the thermohaline circulation's effect on the potential vorticity signature. The *de Szoeke and Chelton* [1999] framework is applied to the observed potential vorticity gradients to provide an estimate of their effect on planetary wave propagation.

2. Data and Methods

Potential vorticity is mapped using conductivity-temperature-depth (CTD) data and high-quality historical bottle data, highlighting many smaller scale features not previously identified. The CTD data include all of the U.S. World Ocean Circulation Experiment (WOCE) Indian Ocean data from 1995-1996 cruises, the National Oceanic and Atmospheric Administration (NOAA) repeat Indian Ocean cruises in 1995, the 1987 32°S cruise, the Australian 1995 WOCE 155°E line, and the French Suzil cruise in 1991. For cruise tracks and information, see http://www-ocean.tamu.edu/WOCE/uswoce.html. The historic bottle data are from the Indian and Pacific Reid-Mantyla data sets [*Mantyla and Reid*, 1995; *Reid*, 1997]. The concurrent use of CTD and bottle data will be discussed below.

Potential vorticity is given by

$$Q = \frac{(f+\xi)}{\rho}\frac{\partial \rho}{\partial z} \tag{1}$$

where f is the planetary vorticity, ξ is the relative vorticity ($v_x - u_y$), and $(1/\rho)\partial\rho/\partial z$ is the stretching term. In large-scale studies where the Rossby number is small, the relative vorticity is negligible in comparison with the other two terms except in strong boundary currents. *Hall* [1994] compared the relative sizes of the potential vorticity terms in the Gulf Stream and concluded that both the relative vorticity and the horizontal vorticity terms (not in equation (1)), which must be included to account for steep isopycnal slopes, are of the same order. Together they comprise as much as 25% of the stretching term. In strong currents, then, our potential vorticity may be in error up to 25%. However, a comparison between the total potential vorticity and $(f/\rho)(\partial\rho/\partial z)$ [*Hall,* 1994] indicates that the patterns are remarkably similar. *Gille* [1997] finds that relative vorticity is negligible even in the strong Antarctic Circumpolar Current (ACC). Therefore the potential vorticity is approximated as $Q \sim (f/\rho)(\partial\rho/\partial z)$ and calculated from hydrographic data. Following *Talley and McCartney* [1982] and *Talley* [1988], the quantity plotted here is $-(f/g)N^2\ 10^{14}$ (cm s)$^{-1}$, where N^2 is the Brunt-Vaisala frequency $-(g/\rho)(\partial\rho/\partial z)$, and the sign of Q is ignored in our figures and plates.

Potential vorticity was plotted on 11 neutral density surfaces chosen to sample the Indian Ocean water masses. Neutral density (γ^n) surfaces were calculated using the code from *Jackett and McDougall* [1997]. Neutral surfaces are the most consistent when the mapping range extends across entire ocean basins and particularly when the range crosses the ACC where isopycnals make large depth excursions [*McDougall,* 1987]. These neutral surfaces are comparable to *Reid*'s [1994, 1997] use of patched σ_θ, σ_1, σ_2, σ_3, and σ_4 surfaces. Our own comparison using Reid's method across the ACC shows the neutral and patched surfaces to be nearly identical. The surfaces are grouped into five vertical layers: Subantarctic Mode Water (SAMW); Antarctic Intermediate Water (AAIW); oxygen minimum layer; Indian Deep Water (IDW), which includes North Atlantic Deep Water (NADW); and Lower Circumpolar Deep Water (LCDW). Layers do not perfectly coincide with water masses, and each map indicates the layer's pressure. Table 1 lists the surfaces, the water masses they best represent, and the approximate pressures and potential densities that they cross for reference. Note that the γ^n surfaces were those considered and do not represent end points of water masses. We have chosen not to consider layers in the upper thermocline that outcrop in the subtropical gyre and are highly affected by monsoonal variability. In the SAMW layer and deeper, monsoonal variability is decreased and geographically isolated to the Somali coast and Indonesian Throughflow [*You,* 1997].

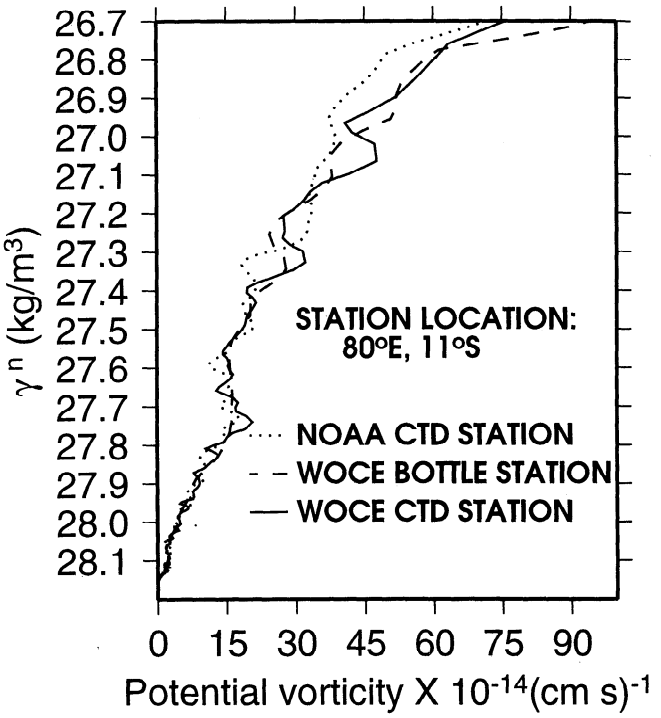

Figure 1. Potential vorticity [10^{-14} (cm s)$^{-1}$] from conductivity-temperature-depth (CTD) and bottle data at 80°E, 11°S. The CTD (solid line) and bottle (dashed line) data were taken simultaneously on the World Ocean Circulation Experiment (WOCE) 80°E line in March 1995. Also shown for comparison is the potential vorticity from a CTD profile (dotted line) at the same location from the National Oceanic and Atmospheric Administration (NOAA) repeat section in October 1995. The location is represented by the dot on Figure 3 at 80°E, 11°S.

Because of the difference in vertical sampling between the CTD and bottle data, the technical calculation of potential vorticity differs. From the 2-dbar CTD data, the potential vorticity is calculated at each sampling point using a Gaussian smoothing with a vertical half

Table 1. Layers of the Indian Ocean

γ^n Layer	Description	Pressure, dbar	Potential Density
26.81 and 26.88	SAMW	250-500	26.73-26.8σ_θ, 31.24-31.5σ_1
27.15 and 27.35	AAIW	500-1400	27.0-27.3σ_θ, 31.51-31.78σ_1
27.60 and 27.74	oxygen minimum layer	1000-2000	32.02-32.2σ_1, 36.69σ_2
27.95, 28.09, and 28.12	IDW	1900-4140	36.9-36.91σ_2, 41.49-41.53σ_3, 45.88-45.89σ_4
28.14 and 28.16	LCDW	3200-4600	41.54-41.56σ_3, 45.91-45.94σ_4

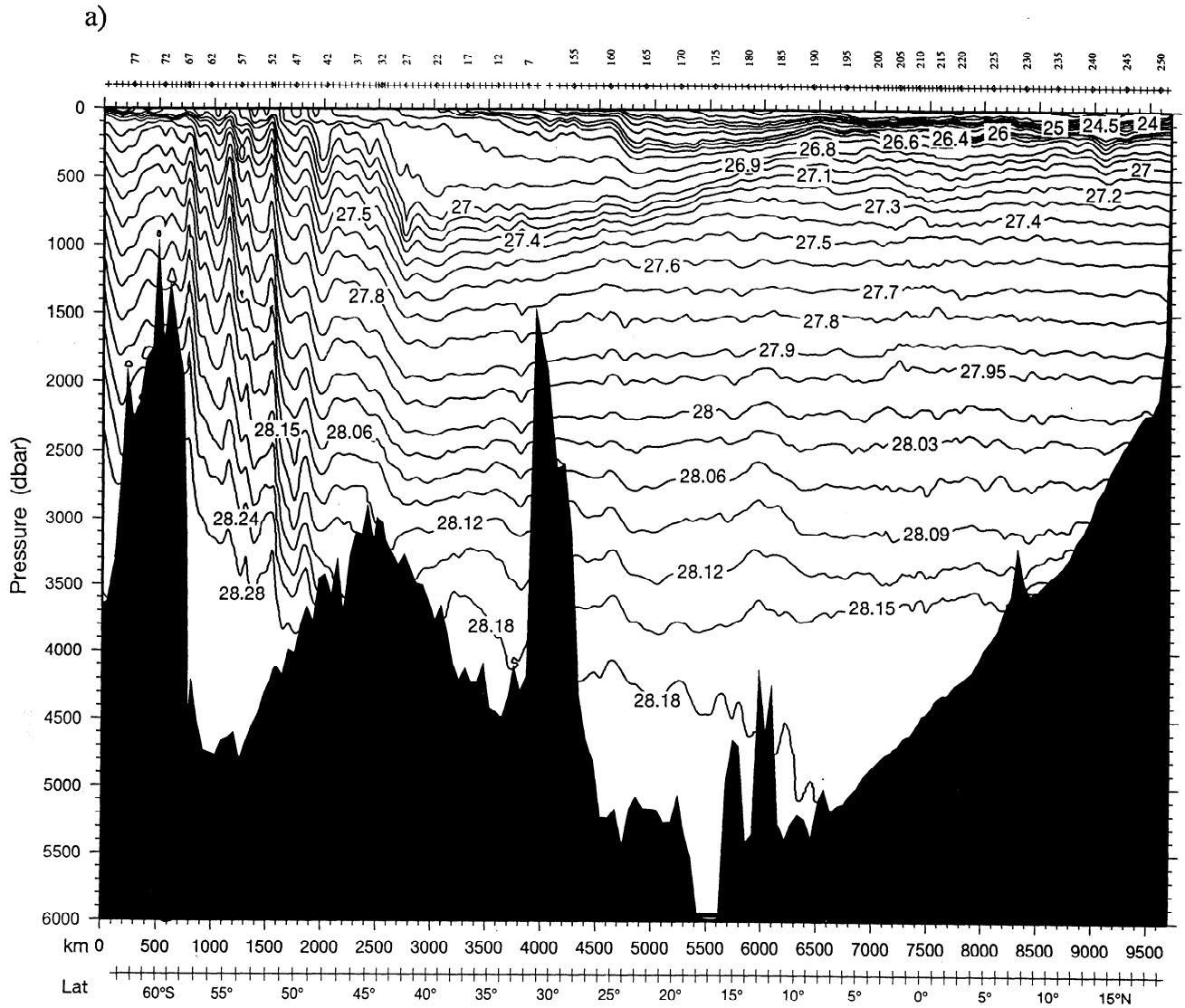

Figure 2. (a) Vertical section of γ^n (kg/m^3) versus pressure (decibars) at 95°E from WOCE sections. (b) Vertical section of potential vorticity [10^{-14} (cm s)$^{-1}$] plotted against γ^n (kg/m^3) at 95°E. See Figure 3 for station track along ~95°E. (c) Vertical section of potential vorticity [10^{-14} (cm s)$^{-1}$] versus pressure (decibars) at 32°S.

width of 50 dbar for the noisy N^2 derivative. Potential vorticity is then output at 20-dbar intervals and linearly interpolated to the desired neutral surfaces. The bottle data sampling is sparser and uneven, with higher resolution in the upper water column where the stratification is greater. Neutral surfaces are calculated from the original bottle data, and then the original data and γ^n are interpolated to 10-dbar intervals using a cubic spline. From this interpolated 10-dbar data, the neutral surfaces and data are linearly interpolated to γ^n levels at an interval of 0.02 kg/m^3. Finally, N^2 and potential vorticity are calculated.

While the sampling difference between bottle and CTD data makes their combined use potentially problematic, comparison between the two fields indicates that they are compatible. Figure 1 shows a representative comparison between the two data types taken at the same location on the same cruise. They are also compared with a CTD profile repeated several months later at the same location (see Figure 3, 80°E, 11°S for location). Figure 1 shows the two data types can be used in combination because their differences are the same order of magnitude as repeat section differences.

The potential vorticity was hand-contoured on 11 γ^n surfaces. Anomalous data points, which were largely due to uneven quality of the bottle data, were ignored. Six surfaces are shown: two representative of different levels of the SAMW and one representative of each of the other four water mass layers listed in Table 1. The remaining five surfaces had most features in common with those displayed here. While temporal variability was not examined, the contourability of data from dif-

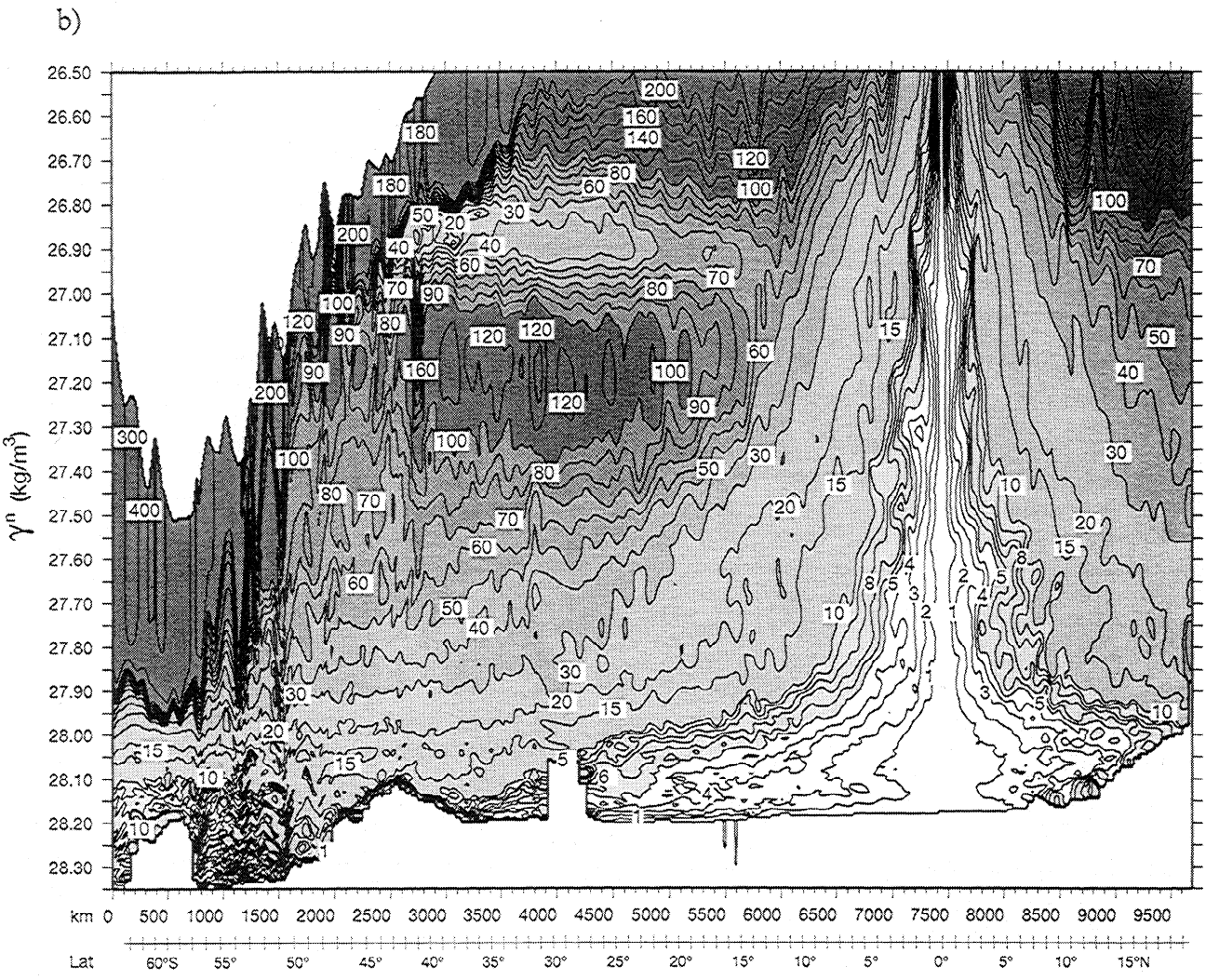

Figure 2. (continued)

ferent seasons and years suggests that the features are robust with respect to monsoonal variability.

Figure 2 shows meridional vertical sections of neutral density (γ^n) versus pressure and potential vorticity versus γ^n from Antarctica to the northern Bay of Bengal along 95°E from WOCE sections and a vertical section of zonal potential vorticity at 32°S (see 95°E and 32°S sections on Figure 3 for location). Figure 2a indicates that the shallowest layer displayed, $\gamma^n = 26.81$, lies at ~300 dbar and that the water column is well covered by the chosen γ^n levels (Table 1). The subtropical gyre is seen in the bowling neutral surfaces, and the ACC's several fronts appear as large vertical neutral surface excursions. In the deep and abyssal waters between 40°S and 45°S, neutral surfaces reverse slope near 3000 dbar. A similar reversal occurs near 4500 dbar at 10°S.

The meridional potential vorticity in Figure 2b and the zonal section of potential vorticity in Figure 2c clearly mark several of the layers. The SAMW is seen as a low potential vorticity intrusion centered at $\gamma^n \sim 26.85$ (~500 dbar), reflecting its nearby surface origin. Below it, the AAIW is a vertical maximum. Strong horizontal gradients dominate near the equator where f goes to zero. Deep and abyssal water masses have no unique potential vorticity signatures such as minima or maxima. Their effect on potential vorticity is apparent from the increased vertical potential vorticity gradient for γ^n greater than 27.90 (Figure 2b) and pressures greater than ~2500 dbar (Figure 2c).

For an ocean at rest the potential vorticity depends on f/h, where h is layer thickness. In the upper ocean, this creates a background potential vorticity gradient which is β, with h constant. On deep surfaces near bathymetry, the background state also depends on bathymetry. Assuming a relatively flat neutral surface at middepth, a measure of resting state potential vorticity that incorporates bathymetry is f/h, where h is the distance from the neutral surface to the bottom. This potential vorticity is high over shallow bathymetry where h is small and low in deep basins where h is large. The assumption of a middepth level where neutral surfaces are nearly flat is appropriate in the Indian

c)

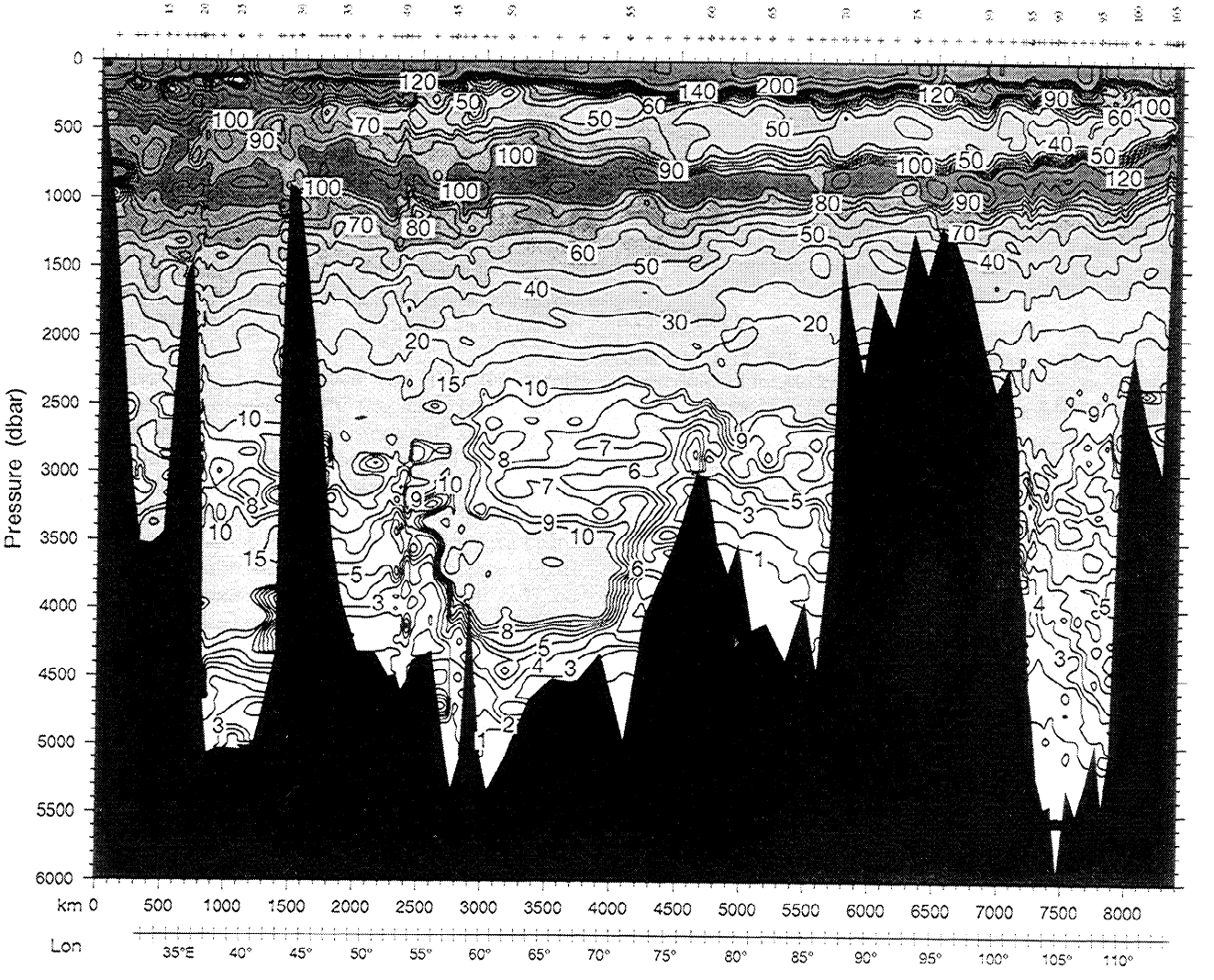

Figure 2. (continued)

Ocean except across the ACC where surfaces make 500- to 1000-m excursions (Figure 2a). The resting bathymetric background state plotted here (Figure 3) uses the neutral surface $\gamma^n = 27.74$, which lies at ~1500 m. Since this surface is not flat across the ACC, the bathymetric potential vorticity is altered slightly by the ACC. The ACC's most obvious modification of the resting bathymetric potential vorticity is that the high associated with the Southeast Indian Ridge (see Figure 4 for location) is shifted slightly northward south of Australia. If the isopycnals were flat, the high would be directly over the ridge. The northward offset arises because the isopycnals directly over the crest of the ridge have already begun their steep ascent north of the ridge, increasing h (see Figure 2). To the northern side of the bathymetric peak, the bottom is shoaling quickly while the isopycnals remain flat. Thus the observed high is centered just north of the ridge where h is a minimum. Resting state, bathymetrically set potential vorticity highs are observed over other ridges (e.g., Ninetyeast Ridge, Madagascar Ridge) in Figure 3.

3. Neutral Surfaces

Three major basins, the Mascarene, Central Indian, and West Australian, are separated by ridges and partition the northern and central Indian Ocean, and an extensive series of ridges and basins is found in the southern Indian and Southern Oceans (Figure 4). The following discussion proceeds from the shallowest surface to the deepest. We do not show any surfaces representative of the upper thermocline.

3.1. Subantarctic Mode Water: Neutral Density $\gamma^n = 26.81$ and 26.88

In the southern Indian Ocean, the SAMW dominates much of the top 500 m of the water column. SAMW is formed as winter cooling leads to convective overturning and the formation of a deep mixed layer just north of the Subantarctic Front [*McCartney,* 1977]. SAMW is then subducted into the thermocline where it becomes part of the Indian Central Water (ICW) [*Sverdrup et al.,* 1942; *Warren,* 1981; *You and Tomczak,*

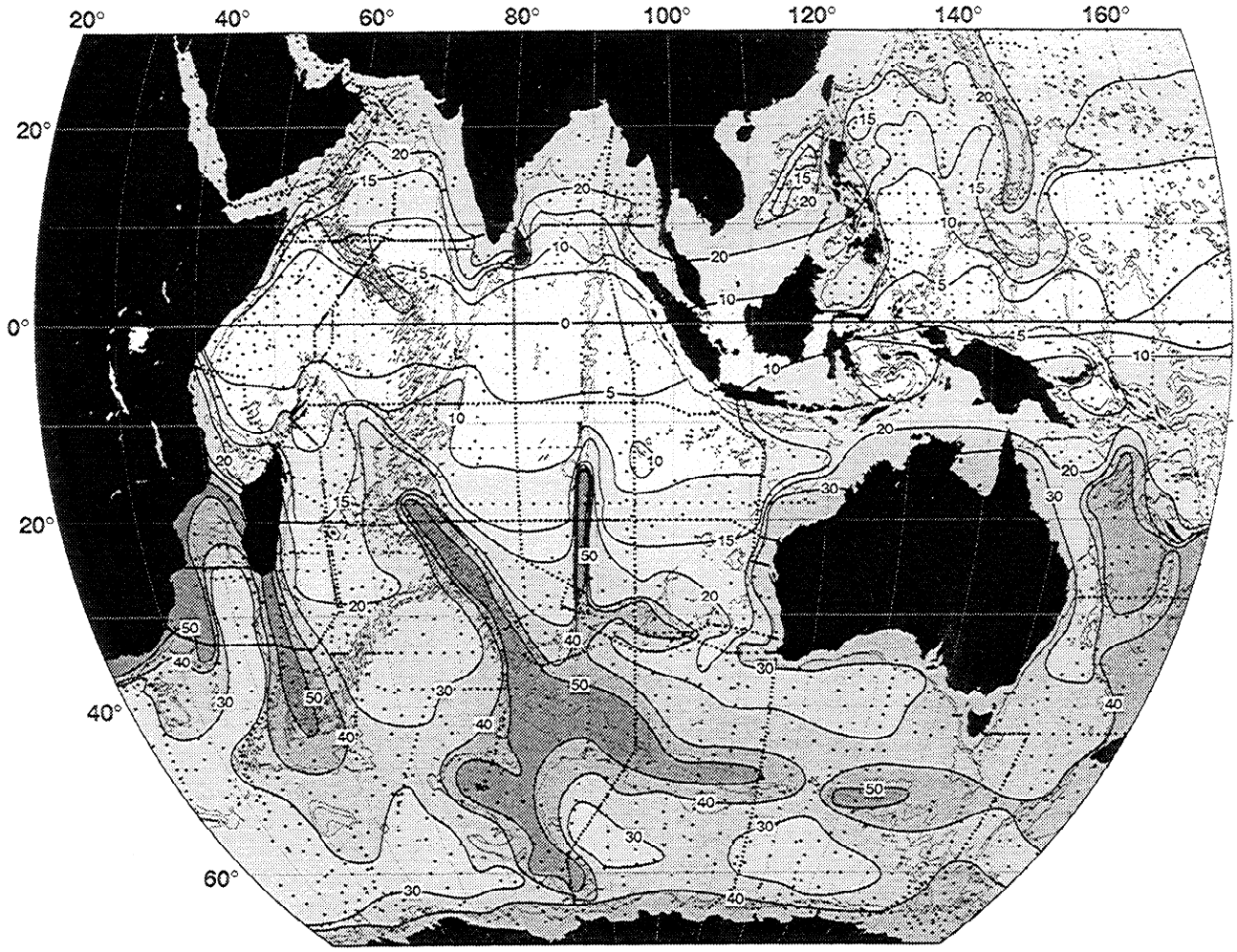

Figure 3. Contour map of background bathymetric potential vorticity [10^{-7} (cm s)$^{-1}$] calculated using the distance from the $\gamma^n = 27.74$ neutral surface to the bottom. The potential vorticity approaches infinity at the coasts (not shown). Black dots are stations used in contouring. See the text for explanation.

1993]. Mode water lends itself well to potential vorticity analysis since it is identified by a weak vertical density/temperature gradient that creates a vertical and lateral potential vorticity minimum. The Indian Ocean SAMW is commonly divided into three density ranges: 26.65-26.7σ_θ, which dominates in the southwestern Indian Ocean; 26.7-26.8σ_θ, which dominates in the central Indian; and 26.8-26.85σ_θ, which dominates in the southeastern Indian [*McCartney,* 1982; *Fine,* 1993]. The lightest-mode water is separated both in physical and density space from the other two types and is associated with the Agulhas circulation [*McCartney,* 1982; *Fine,* 1993]. The two surfaces that are shown here, $\gamma^n = 26.81$ and $\gamma^n = 26.88$, intersect the intermediate and dense varieties of the SAMW.

Contained in the SAMW layer are the Indonesian Throughflow Water (also called the Australasian Mediterranean Water [*You and Tomczak,* 1993]), the Persian Gulf outflow water, and the North Indian Central Water (aged ICW/SAMW [*You and Tomczak,* 1993]). The Indonesian Throughflow Water is a low-salinity, surface-intensified feature that is advected westward along 10°S to Madagascar. Persian Gulf Water is the shallow high-salinity water mass in the Arabian Sea. Large river runoff and excess of precipitation over evaporation create a fresh surface layer in the Bay of Bengal. The strong halocline below this fresh layer lies at the top of the surfaces we consider. Near Somalia, this layer is strongly affected by seasonally reversing currents and seasonal upwelling.

On $\gamma^n = 26.81$ (Plate 1a), from 10°S to 10°N in the tropics, potential vorticity is β-dominated. In the Arabian Sea, the outflow from the Persian Gulf creates a southward tongue of high potential vorticity similar to the high-salinity tongue on comparable surfaces given by *You and Tomczak* [1993]. The river outflows in the Bay of Bengal create a strong halocline which shows up as a tongue of higher potential vorticity below the outflow. Shallow isopycnal layers (lighter than those here) of *Keffer* [1985] show similar patterns.

The rest of the map shows potential vorticity dominated by the circulation of source waters in the basin.

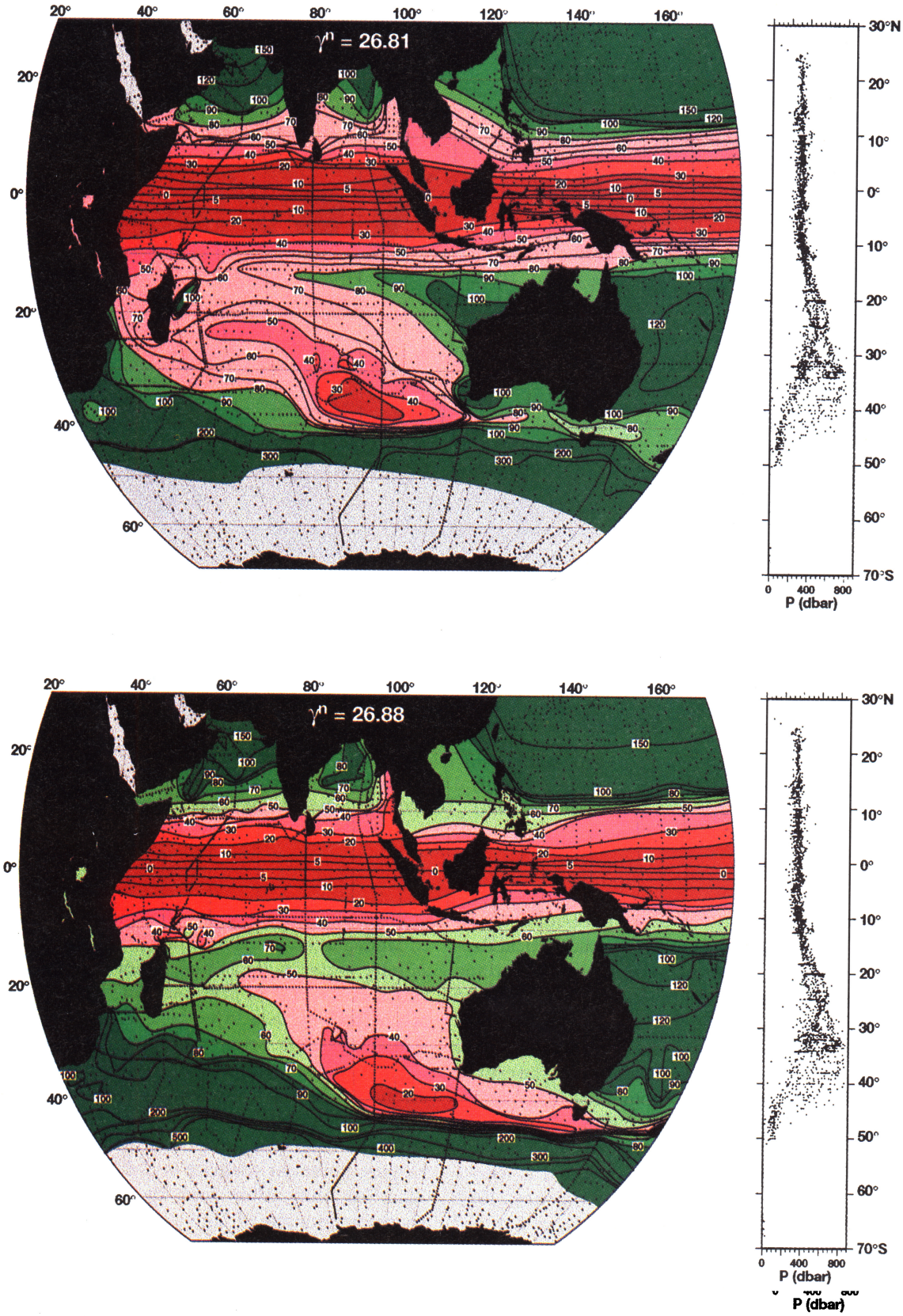

Plate 1. Contour map of potential vorticity $[10^{-14}$ (cm s)$^{-1}]$ plotted on (a) the $\gamma^n = 26.81$ surface and (b) the $\gamma^n = 26.88$ surface in the Subantarctic Mode Water (SAMW) layer. Green indicates highs, and red indicates lows. Grey shading marks the edge of the neutral surface. Shown to the right is pressure as a function of latitude on the respective surfaces.

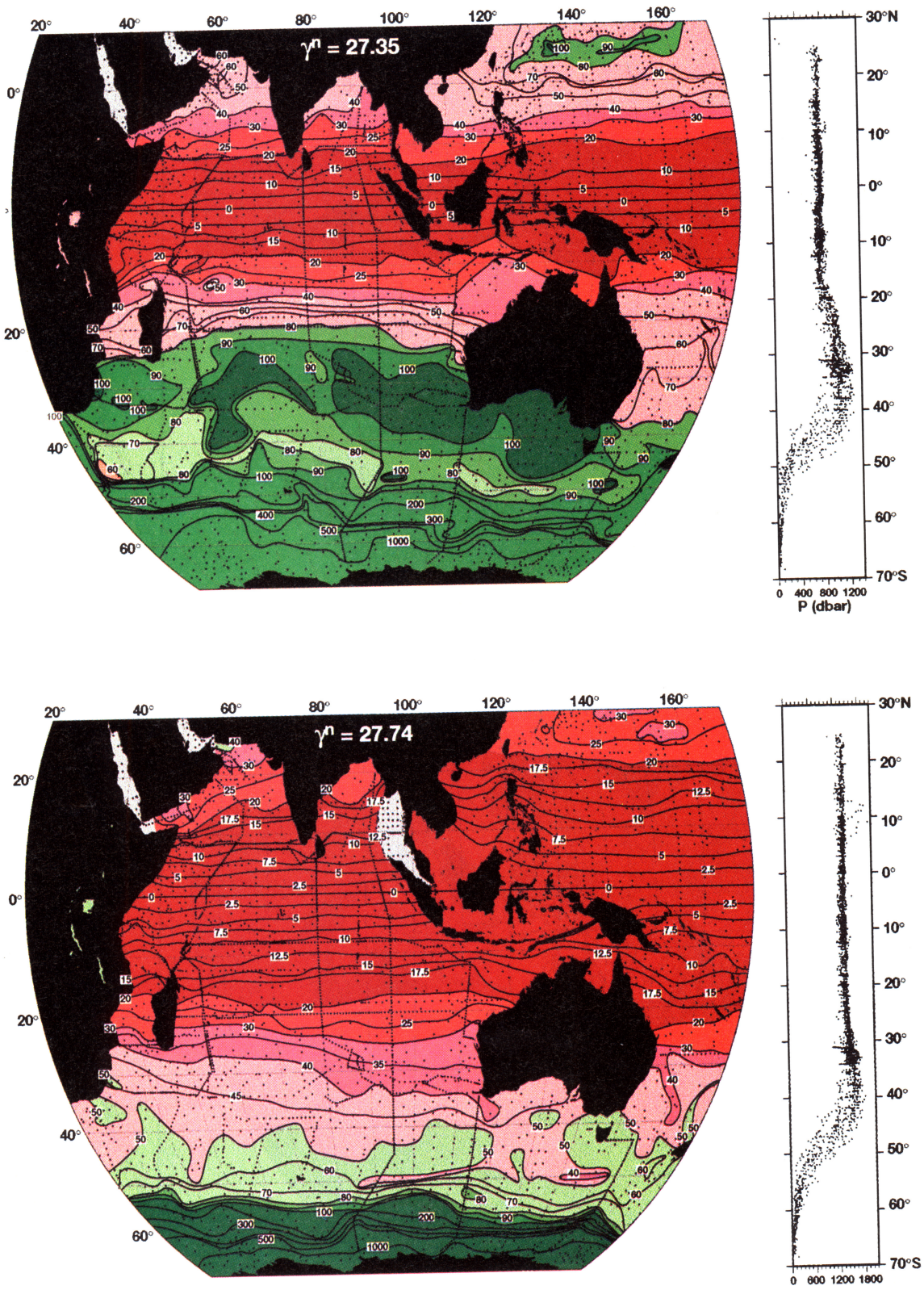

Plate 2. Contour map of potential vorticity [10 $^{-}$ (cm s) $^{-}$] plotted on (a) the γ ^{n} = 27.35 surface in the Antarctic Intermediate Water (AAIW) layer and (b) the γ^n = 27.74 surface in the oxygen minimum layer. Green indicates highs, and red indicates lows. Grey shading marks the edge of the neutral surface. Shown to the right is pressure as a function of latitude on the respective surfaces.

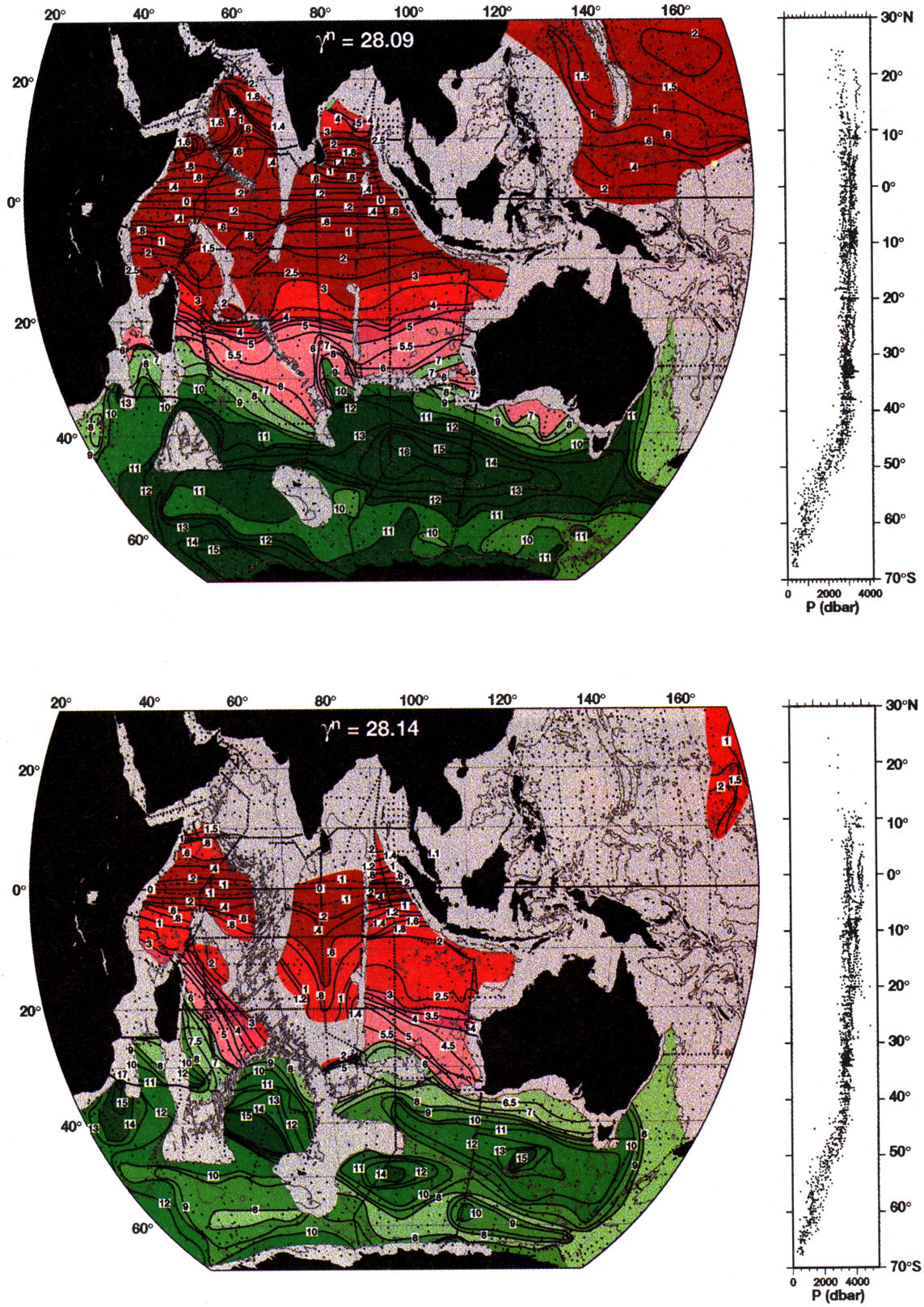

Plate 3. Contour map of potential vorticity [10^{-14} (cm s)$^{-1}$] plotted on (a) the $\gamma^n = 28.09$ surface in the Indian Deep Water (IDW) layer with the 3000-m isobath and (b) the $\gamma^n = 28.14$ surface in the Lower Circumpolar Deep Water (LCDW) layer with the 3500-m isobath. Green indicates highs, and red indicates lows. Grey shading marks the edge of the neutral surface. Shown to the right is pressure as a function of latitude on the respective surfaces.

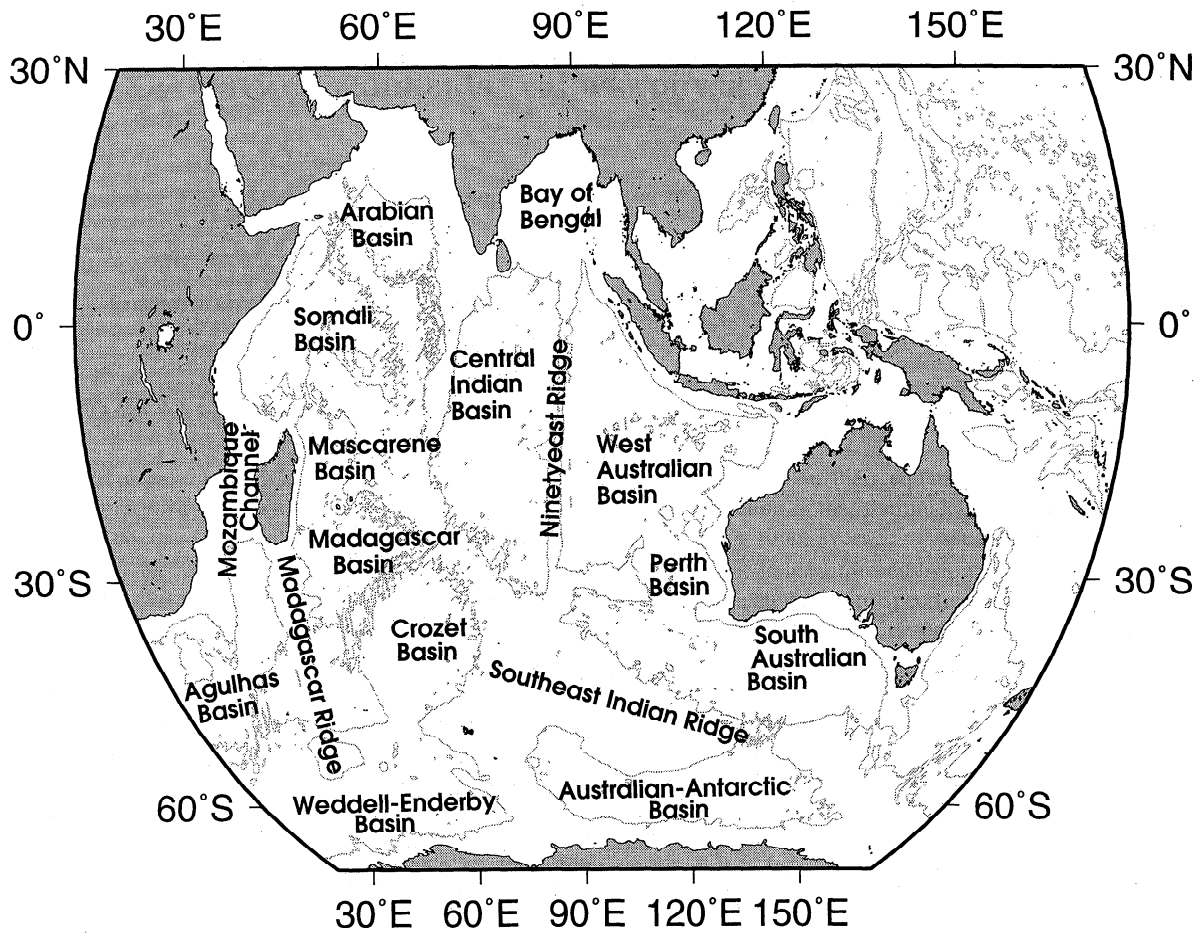

Figure 4. Major basin and ridge systems of the Indian and Southern Oceans plotted with the 4000-m isobath.

The β-dominated pattern of the tropics is interrupted at 10°S by a zonal ridge of high (green) potential vorticity. The influence of this high extends westward to within 10° of Madagascar as it is carried by the South Equatorial Current. The high potential vorticity signal originates off the northwest coast of Australia at the Exmouth Plateau and curves north with the gyral circulation. As it reaches 10°S, the high signal appears to be picked up and carried by the Indonesian Throughflow jet. The Indonesian Throughflow Water might be expected to have its own high potential vorticity signal due to its constricted entrance into the Indian Ocean. However, the signal suggests that the β-effect dominates any decrease in isopycnal spacing. The β-effect also overwrites the Somali Current's signature on potential vorticity. The low signature of SAMW (red) originates near the southwest corner of Australia and curves to the north and west following the circulation of the subtropical gyre. *Keffer*'s [1985] map for the layer σ_θ = 26.5-27.0 also shows a low in the subtropical gyre.

Plate 1b (γ^n = 26.88) crosses the densest variety of the SAMW. Its origin south of Australia is evident from the low which extends south of Australia and throughout the return circulation of the gyre. On both of the surfaces in this layer, the SAMW is coincident with the wind-driven gyre. However, the lower gradients there appear to be caused primarily by the common source water. Homogenization in a western shadow zone is not seen. Most of the basin is β-dominated outside of the gyre. A low near 25°E, 37°S appears on both this level and on γ^n = 26.81. This may be an Agulhas eddy.

Figure 5 shows the γ^n value of the vertical potential vorticity minimum in the γ^n range 26.0-27.35. It clearly depicts the separation in physical and density space between the lighter-mode water in the southwest and the heavier-mode water in the southeast. The lighter-mode water is on the warm side of the Agulhas Retroflection, which merges with the Subantarctic Front. Therefore this variety of mode water has both subtropical and subpolar influence. South of Australia, the minimum potential vorticity lies near γ^n = 27.0, which is the densest variety of SAMW in the Indian Ocean [*McCartney,* 1982; *Fine,* 1993]. On the northern edge of Antarctica, the potential vorticity minimum lies outside the SAMW density range with γ^n greater than 27.2, but this water is well separated from the SAMW formation region by the ACC. The low potential vorticity here is likely formed by deep winter mixed layers. At most,

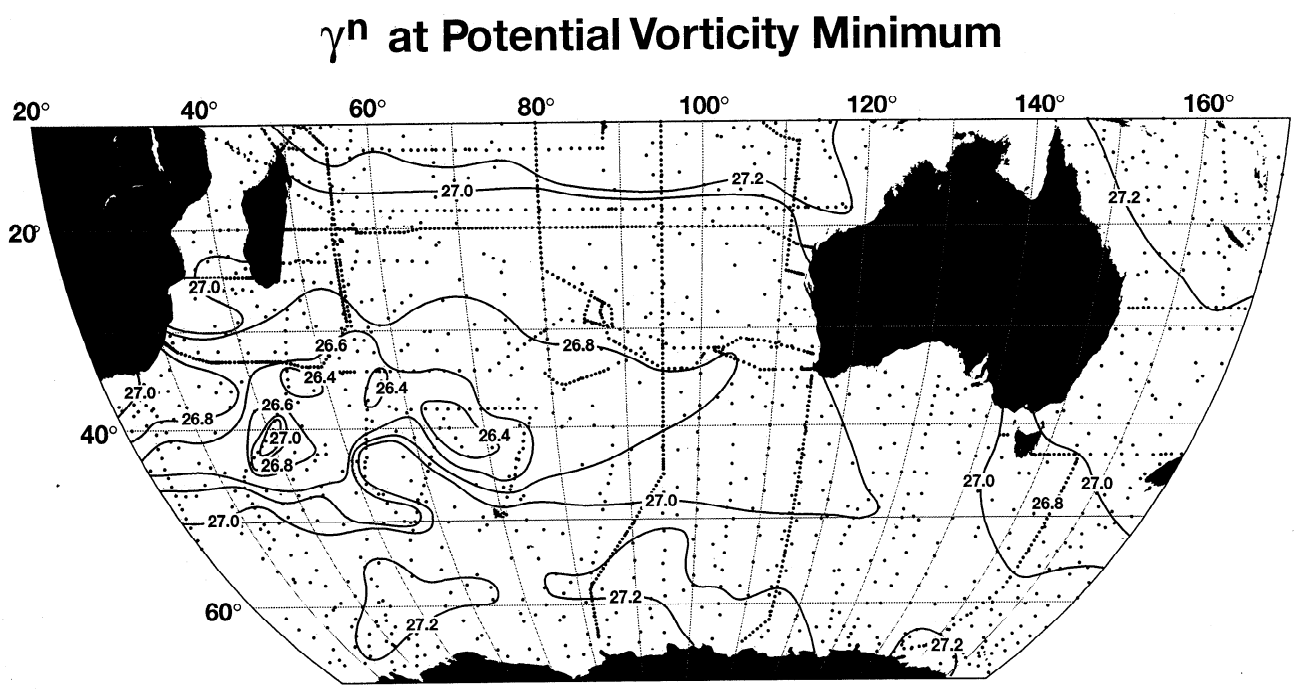

Figure 5. Contour map of the γ^n value (kg/m^3) where potential vorticity is a minimum in the γ^n = 26.0-27.35 range.

only minimal amounts of the water within these mixed layers cross the ACC. To the north, the density of the potential vorticity minimum also increases as the minimum is eroded away from above by the high potential vorticity carried by the Indonesian Throughflow Water.

3.2. Antarctic Intermediate Water: Neutral Density γ^n = 27.15 and 27.35

The next levels were chosen to represent AAIW, the low-salinity water mass present in each of the three southern oceans. In the Indian Ocean, the core of this salinity minimum lies near 27.2σ_θ and ranges between 27.1 and 27.3σ_θ [*Fine*, 1993]. In a comprehensive study of the AAIW using CFCs, *Fine* [1993] identified its major circulation pathways in the Indian Ocean. The main and most northward injection occurs between 60°E and 64°E, with other injections between 35°E and 50°E and in the southeast Indian basin from south of Australia. CFC ages indicate that the latter AAIW may have first circulated in the South Pacific before traveling westward into the Indian.

In the AAIW layer, Red Sea Water dominates the Arabian Sea and crosses the equator in the Mozambique Channel, and its high salinity signature is interspersed with AAIW in the Agulhas and the Agulhas Retroflection [*Fine et al.*, 1988]. The Leeuwin Current flows south along the northwest coast of Australia. The subtropical gyre and Agulhas Current are still active in these layers [*Gordon et al.*, 1987].

AAIW is a vertical maximum in potential vorticity between the low potential vorticity mode water above and the low potential vorticity deep water below (see Figure 2b). Whereas the Atlantic AAIW has a low potential vorticity signal upon leaving its formation region in the southwest Atlantic, the Indian Ocean is too far downstream to maintain this signature [*Talley*, 1996]. On γ^n = 27.35 (Plate 2a) as on the 31.7σ_1 isopycnal shown by *Talley* [1996], the three main pathways identified by *Fine* [1993] are apparent. An extensive high originating south of Australia enters the return arm of the gyre. It is most likely locally generated south of Australia as the AAIW circulates northward and westward into the Pacific Ocean from its eastward traverse along the Subantarctic Front from the Atlantic [*Talley*, 1996]. The second high near 65°E has the most northern extent, and a third hugs the southeast coast of Africa. This supports the idea of exchange between the Indian and Atlantic [*Fine et al.*, 1988; *Gordon et al.*, 1992; *Talley*, 1996] since the Agulhas runs through this pocket of AAIW. Similar to the SAMW, the AAIW is found in the subtropical gyre region, where gradients are also reduced. Once again, the reduced gradients appear to be primarily the result of the common source waters. *You and McDougall* [1990] map potential vorticity on the γ^n = 27.25 surface and show the central and eastern high as well and the banded low farther south, as does *Keffer* [1985] on σ_θ= 27.0-27.3. *Keffer* [1985] attributes the zonal low to a data artifact, while both *Talley*'s [1996] analysis based on limited data and the new data suggest that it is a robust feature. This potential vorticity low corresponds to the region of higher γ^n north of Antarctica seen in Figure 5.

The tropical and northern parts of this surface are β-dominated. The Red Sea Water has no potential vor-

ticity signature due to its proximity to the equator. The isopleths that tilt to the south against the western coast of Australia may be due to the southeastward Leeuwin Current.

3.3. Oxygen Minimum Layer: Neutral Density γ^n = 27.60 and 27.74

The oxygen minimum layer has no Indian Ocean sources. It lies near 1500 m, mostly outside of the influence of the wind-driven circulation [*Reid,* 1981; *Toole and Warren,* 1993]. Plate 2b, γ^n = 27.74, shows that isopleths in this layer generally follow latitude circles, indicating β-domination. *You and McDougall* [1990] show potential vorticity at γ^n = 27.5, where the influences of both the more homogenized AAIW layer above and the β-dominated oxygen minimum layer below can be seen. The expected pattern is β-domination on a level that is outside the wind-driven influence and that has no direct water mass sources (see Figure 2). Therefore we choose this surface for our calculation of the background potential vorticity for the abyssal ocean (section 2).

3.4. Indian Deep Water: Neutral Density γ^n = 27.95, 28.09, and 28.12

In this layer, thermohaline circulation plays a determining role in the distribution of potential vorticity. This layer encompasses the warm and salty NADW that enters south of Africa [*Mantyla and Reid,* 1995] and which is constrained to the Mozambique Channel with only a small overflow through the Madagascar Ridge to the western Madagascar Basin [*Toole and Warren,* 1993]. Deep water enters the three main basins in deep western boundary currents and circulates in a generally cyclonic sense. In the Southern Ocean, cyclonic gyres have been identified in both the Weddell-Enderby and the Australian-Antarctic Basins [*Park and Gamberoni,* 1995]. A cyclonic circulation is also established south of Australia where an eastward flow against the coast is returned westward just south of 40°S [*Hufford et al.,* 1997].

The potential vorticity observed on γ^n = 28.09 (Plate 3a) clearly shows the deep waters entering the basins. In the Crozet and Madagascar Basins, the isopleths tilt to the northeast. The tilting is especially strong in the Crozet Basin as Circumpolar Deep Water moves northward in the west while North Indian Deep Water flows southward in the east [*Park et al.,* 1993; *Toole and Warren,* 1993]. Tongues of high potential vorticity move north into the Mozambique Channel and the Central Indian Basin. Although this plate does not show any strong alteration of the isopleths due to inflow into the West Australian Basin, the other mapped surfaces (γ^n = 27.95 and 28.12) in this layer do (not shown). Deep water can also be seen entering the Arabian Basin. The gradients are lower in the Weddell-Enderby and Australian-Antarctic Basins, which may be due to homogenization by the gyres observed there.

A comparison between the bathymetric resting potential vorticity (Figure 3) and the observed potential vorticity is useful for these deep surfaces. The observed potential vorticity (higher in the basins, lower over topography) is the reverse of the bathymetric pattern, suggesting that it is not bathymetrically controlled. The pattern south of Australia (from north to south) of low-high-low is the only feature which appears to be highly influenced by bathymetry. However, the circulation here still plays a strong role. The topographic high should be centered right over the ridge, but the ACC appears to have shifted the high to the north. The northward shift is due to the vertical divergence of neutral surfaces near 40°S in the deep ocean, as described (see section 2).

These patterns differ from those observed by *O'Dwyer and Williams* [1997]. In this layer, they observed a mostly β-dominated structure, and any deviations were within their error limits. This discrepancy can be explained by the new high-resolution data used in our study and by our avoidance of smoothing bias by using hand contouring.

3.5. Lower Circumpolar Deep Water: Neutral Density γ^n = 28.14 and 28.16

Potential vorticity in this layer is very similar to that of the IDW. However, topography partitions the basins more completely at these depths. LCDW enters the Crozet/Madagascar and West Australian Basins in deep western boundary currents. The Central Indian Basin is isolated except for a couple of deep sills in the Ninetyeast Ridge. The main overflow occurs at 11°S [*Warren,* 1982; *Mantyla and Reid,* 1995] with a smaller one at 28°S [*Toole and Warren,* 1993; *McCarthy et al.,* 1997]. The Weddell-Enderby, Australian-Antarctic, and South Australian Basins exhibit cyclonic circulations [*Park and Gamberoni,* 1995; *Hufford et al.,* 1997].

The γ^n = 28.14 surface was chosen to represent this layer (Plate 3b). Active meridional circulation determines the potential vorticity pattern. The isopleths of the Crozet and Madagascar Basins tilt very strongly to the northeast as the western boundary current carries in bottom water. The isopleths of salinity and oxygen in this layer of the Crozet Basin also exhibit a similar orientation [*Park et al.,* 1993]. Bottom water entering the West Australian Basin also tilts isopleths to the northeast. In the Central Indian Basin, the 28°S overflow [*McCarthy et al.,* 1997] is apparent as a relative low, as is the 11°S overflow. The southward spreading tongue of low potential vorticity in the Central Indian Basin probably reflects the spreading of the overflow water there [*Warren,* 1982]. The gradients are again slightly lower in the Weddell-Enderby and Australian-Antarctic Basins. The bathymetric low-high-low pattern south of

Australia still appears, as in the IDW layer, with the high offset to the north.

These patterns in the deep and abyssal waters, which differ markedly from both the β-dominated and bathymetric potential vorticity, indicate a strong meridional circulation in the deep Indian Ocean. Tilted potential vorticity contours and tongues show that deep water is entering the western side of the basins. These signatures indicate the flow's strength, since isoneutral surfaces have been altered so that meridional flow does not cross potential vorticity isopleths [*O'Dwyer and Williams,* 1997].

4. Geographical Areas

A brief top-to-bottom description of the potential vorticity in the main geographic areas of the Indian Ocean serves to both summarize and give a better three-dimensional picture of the structure.

4.1. Tropics

For the upper and intermediate layers of the Indian Ocean, the potential vorticity field is β-dominated in tropical latitudes between 10°S and 15°N. The potential vorticity gradient changes sign at the southern edge of the region of β-domination (Figure 2b near 15°S), which allows for instability and corresponds to the increased variability observed by *Stammer* [1997]. Approaching the equator, potential vorticity becomes vanishingly small as f goes to zero. In the upper layers, this effect dominates any change in h, which is relatively negligible. In the deep and abyssal waters, however, the region of β-domination shrinks to within 5° of the equator. For a substantial region of the tropics, the deep flow is strong enough to cause an alteration in h which is of the same order as the decrease in f. The most salient alteration from β occurs on $\gamma^n = 28.14$ (Plate 3b) where there is evidence of southward flow in the Central Indian Basin.

4.2. Northern Indian Ocean

The northern Indian Ocean contains the Arabian Sea and the Bay of Bengal and is bordered to the south by the tropics. These areas exhibit potential vorticity patterns altered from β by flow at many of their depths. In the upper layers, the outflow waters and the increased gradients associated with them bow the isopleths southward. In the intermediate waters, the β pattern resumes. Deeper in the water column, the Arabian Sea shows some perturbation by deep water inflow (Plate 3a) while the other layers remain β-dominated. The area of the Bay of Bengal quickly shrinks with depth, and the portion that contains deep surfaces remains β-dominated.

4.3. Western Indian Ocean

The western Indian Ocean is defined here as the basins north of ~40°S and west of ~70°E, including the Madagascar, Mascarene, and Crozet Basins and the Mozambique Channel. The upper layers of the ocean show potential vorticity set by circulating source waters. Both the SAMW and the Indonesian Throughflow Water extend this far west. Near the east coast of Madagascar, the irregular pattern in the upper layers may be due to the South Equatorial Current splitting, with one branch going north and the other south, and/or the strong seasonal differences found there [*You,* 1997]. While the data off the coast of Africa (south of the Mozambique Channel) are somewhat sparse, the potential vorticity pattern shows some suggestion of southward modification by the Agulhas (Plates 1a and 1b). AAIW has a very strong signal in this portion of the ocean. Its high potential vorticity has relatively lower gradients and borders the west coast of Africa with another northward intrusion between 60°E and 80°E.

Waters in the oxygen minimum layer show β-domination, while deep waters have highly tilted (NW-SE) potential vorticity contours. The Crozet, Madagascar, and Mascarene Basins show the most noticeable potential vorticity signature due to the inflow of abyssal water in deep western boundary currents. On deep levels, the isopleths are nearly meridional, and this pattern persists to the bottom. The severity of the tilting here suggests this western arm of the deep western boundary currents may be more active than those entering the Central Indian and West Australian Basins.

4.4. Eastern Indian Ocean

The eastern Indian includes the southern portions of the Central Indian and West Australian Basins as well as the Perth Basin. The upper layers show potential vorticity as a tracer of source waters circulating in the subtropical gyre. High potential vorticity originates off the northwest coast of Australia and is advected westward just south of the Indonesian Throughflow in the north, and low potential vorticity marks the SAMW in the south. These water masses and the potential vorticity signatures they carry enter the gyre's circulation (Plate 1). Deeper, the AAIW also enters from the south and moves in the general direction of the return flow. In these layers, the potential vorticity has weak meridional gradients within the gyre. Plates 1 and 2a show the area south of Australia to be the source of these two subpolar water types in the eastern Indian. Potential vorticity in the eastern Indian becomes β-dominated at middepths. At depth, the deep western boundary currents are clearly seen in the potential vorticity structure.

4.5. Southern Ocean

The Southern Ocean provides source waters to the Indian Ocean and includes the South Australian, Weddell-Enderby, and Australian-Antarctic Basins and the ACC. In the top layers of the South Australian Basin, the SAMW causes the potential vorticity to be low, and directly below it the potential vorticity is high due to the AAIW. In the deep and bottom waters, the poten-

Table 2. Three-Layer Model Parameters

Layer	Bounding Surfaces	Average γ^n	Layer Thickness, m	
			At 20°S	At 30°S
1	surface - $\gamma^n = 26.8$	26.0	400	450
2	$\gamma^n = 26.8 - 27.6$	27.2	700	850
3	$\gamma^n = 27.6$ - bottom	27.9	3400	2900

tial vorticity pattern in the South Australian Basin and over the Southeast Indian Ridge reflects the interaction of the ACC with topography. South of Australia, between 120°E and 140°E and north of ~40°S, a low is apparent and persists to the bottom. The abyssal potential vorticity that might be found in a resting state (Figure 3) shows that the shape and extent of the observed low is topographic. The low extends from the 3500-m isobath south of Australia to 40°S-45°S and is centered over the deepest portion of the South Australian Basin (37°S-45°S). The southern limit of the low moves northward with depth associated with the northern slope of the Southeast Indian Ridge. South of the low is a potential vorticity high centered just north of the shallowest part of the Southeast Indian Ridge. The Subantarctic Front lies over the ridge [*Orsi et al.*, 1995], and this combined with the spreading neutral surfaces shifts the high northward as described above.

South of the Subantarctic Front, the potential vorticity contours of near-surface layers follow the Circumpolar Current. In the AAIW layer, isopleths still follow the current, but a low is found south of the AAIW high. The low is approximately bounded to the north and south by the Subtropical and Subantarctic Fronts, respectively [*Orsi et al.*, 1995], and originates in the South Atlantic [*Talley*, 1996]. On the deepest layers considered, ridges divide the Southern Ocean. The salient features here are the somewhat homogenized pools in the Weddell-Enderby and the Australian-Antarctic Basins associated with the gyres found there.

5. Effect of Potential Vorticity on Rossby Wave Propagation

The above results and discussion have shown that a layer of potential vorticity with lower gradients exists in the Indian Ocean's subtropical gyre, and its existence lends itself to the application of *de Szoeke and Chelton*'s [1999] three-layer model. In the model, the middle layer has homogenized potential vorticity. We are approximating it by a layer with lower meridional gradients. This layer encompasses the SAMW and the AAIW, with the higher-gradient surface waters above and the higher-gradient deep waters below. In order to calculate the change in phase speed using the model, one must know the approximate thicknesses and average densities of the three layers. The layer boundaries and average densities were chosen to represent the layers of differing meridional potential vorticity gradients (Table 2). The thicknesses of the layers vary meridionally, and two examples of thicknesses chosen for the model at 30°S and 20°S are also shown in Table 2. The phase speeds predicted are ~1.3 times greater than those predicted from the standard theory of $c = -\beta\lambda^2$. Here λ is the first baroclinic Rossby radius of deformation, and for the calculation, its values were taken from *Chelton et al.* [1998].

6. Conclusions

The Indian Ocean's potential vorticity distribution is strongly influenced by its many source waters. At depth, the intricate bathymetry gives rise to several deep western boundary currents whose signatures are seen in the potential vorticity. For the upper layers in the subtropical gyre region, the common source waters seem to be the main cause of the lower gradients of potential vorticity. Homogenization in a western shadow region is not observed. The β-effect dominates that of the Somali Current and the Red Sea Water on the potential vorticity field. At intermediate depths, β dominates suggesting the absence of both wind-driven circulation and source waters. In the deep and abyssal ocean, the potential vorticity is different from both β and bathymetric control, indicating strong meridional flow. Since these modifications are not due to bathymetry, thermohaline flow strong enough to cause an isopycnal thickness change of the same magnitude as the change in planetary vorticity is required. These distributions of potential vorticity and its gradients imply that Rossby waves will travel ~1.3 times faster than predicted by standard theory.

Acknowledgments. This study was made possible by the U.S. WOCE Indian Ocean cruises, Australian WOCE P11A, the French Suzil cruise, and the Reid-Mantyla bottle data set. Thanks to Baringer, Bray, Church, Ffield, Gordon, Johnson, McCartney, Molinari, Morrison, Nowlin, Olson, Park, Rintoul, Toole, and Warren for collecting the data and making it available to us. This work was supported by NSF grant OCE-9413160, which also supported the collection of WOCE data along 80°E and 32°S. M.C.M. was funded by a National Defense Science and Engineering Graduate fellowship.

References

Chelton, D. B., and M. G. Schlax, Global observations of oceanic Rossby waves, *Science, 272,* 234-238, 1996.

Chelton, D. B., R. A. de Szoeke, M. G. Schlax, K. el Naggar, and N. Siwertz, Geographical variability of the first baroclinic Rossby radius of deformation, *J. Phys. Oceanogr., 28,* 433-460, 1998.

de Szoeke, R. A., and D. B. Chelton, The modification of long planetary waves by homogeneous potential vorticity layers, *J. Phys. Oceanogr., 29,* 500-511, 1999.

Dewar, W. K., On the potential vorticity structure of weakly ventilated isopycnals: A theory of subtropical mode water maintenance, *J. Phys. Oceanogr., 16,* 1204-1216, 1986.

Dewar, W. K., On "too fast" baroclinic planetary waves in the general circulation, *J. Phys. Oceanogr., 28,* 1739-1758, 1998.

Fine, R. A., Circulation of Antarctic Intermediate Water in the South Indian Ocean, *Deep Sea Res. Part I, 40,* 2021-2042, 1993.

Fine, R. A., M. J. Warner, and R. F. Weiss, Water mass modification at the Agulhas Retroflection: Chlorofluoromethane studies, *Deep Sea Res., 35,* 311-332, 1988.

Gille, S. T., Why potential vorticity is not conserved along mean streamlines in a numerical Southern Ocean, *J. Phys. Oceanogr., 27,* 1286-1299, 1997.

Gordon, A. L., J. R. E. Lutjeharms, and M. J. Gründlingh, Stratification and circulation at the Agulhas Retroflection, *Deep Sea Res., 34,* 565-600, 1987.

Gordon, A. L., R. F. Weiss, W. M. Smethie, and M. J. Warner, Thermocline and intermediate water communication between the South Atlantic and Indian Oceans, *J. Geophys. Res., 97,* 7223-7240, 1992.

Hall, M. M., Synthesizing the Gulf Stream thermal structure from XBT data, *J. Phys. Oceanogr., 24,* 2278-2287, 1994.

Holland, W. R., T. Keffer, and P. B. Rhines, Dynamics of the oceanic general circulation: The potential vorticity field, *Nature, 308,* 698-705, 1984.

Hufford, G., M. S. McCartney, and K. Donohue, Northern boundary currents and adjacent recirculations off southwestern Australia, *Geophys. Res. Lett., 24,* 2797-2800, 1997.

Jackett, D. R., and T. J. McDougall, A neutral density variable for the world's oceans, *J. Phys. Oceanogr., 27,* 237-263, 1997.

Keffer, T., The ventilation of the world's oceans: Maps of the potential vorticity field, *J. Phys. Oceanogr., 15,* 509-523, 1985.

Killworth, P. D., D. B. Chelton, and R. D. de Szoeke, The speed of observed and theoretical long extratropical planetary waves, *J. Phys. Oceanogr., 27,* 1946-1966, 1997.

Luyten, J. R., J. Pedlosky, and H. Stommel, The ventilated thermocline, *J. Phys. Oceanogr., 13,* 292-309, 1983.

Mantyla, A. W., and J. L. Reid, On the origins of deep and bottom waters of the Indian Ocean, *J. Geophys. Res., 100,* 2417-2439, 1995.

McCarthy, M. C., L. D. Talley, and M. O. Baringer, Deep upwelling and diffusivity in the southern Central Indian Basin, *Geophys. Res. Lett., 24,* 2801-2804, 1997.

McCartney, M. S., Subantarctic Mode Water, in *A Voyage of Discovery,* edited by M. Angel, pp. 103-119, Pergamon, Tarrytown, N.Y., 1977.

McCartney, M. S., The subtropical recirculation of mode waters, *J. Mar. Res., 40,* suppl., 427-464, 1982.

McDougall, T. J., Neutral surfaces, *J. Phys. Oceanogr., 17,* 1950-1964, 1987.

McDowell, S., P. Rhines, and T. Keffer, North Atlantic potential vorticity and its relation to the general circulation, *J. Phys. Oceanogr., 12,* 1417-1436, 1982.

O'Dwyer, J., and R. G. Williams, On the potential vorticity distribution in the abyssal waters over the global ocean, *J. Phys. Oceanogr., 27,* 2488-2506, 1997.

Orsi, A. H., T. Whitworth III, and W. D. Nowlin Jr., On the meridional extent and fronts of the Antarctic Circumpolar Current, *Deep Sea Res., Part I, 42,* 641-673, 1995.

Park, Y.-H., and L. Gamberoni, Large-scale circulation and its variability in the south Indian Ocean from TOPEX/POSEIDON altimetry, *J. Geophys. Res., 100,* 24,911-24,929, 1995.

Park, Y.-H., L. Gamberoni, and E. Charriaud, Frontal structure, water masses, and circulation in the Crozet Basin, *J. Geophys. Res., 98,* 12,361-12,385, 1993.

Pedlosky, J., and W. R. Young, Ventilation, potential-vorticity homogenization, and the structure of the ocean circulation, *J. Phys. Oceanogr., 13,* 2020-2037, 1983.

Reid, J. L., On the mid-depth circulation of the world ocean, in *Evolution of Physical Oceanography,* edited by B. A. Warren and C. Wunsch, pp. 70-111, MIT Press, Cambridge, Mass., 1981.

Reid, J. L., On the total geostrophic circulation of the North Atlantic, *Prog. Oceanogr., 33,* 1-92, 1994.

Reid, J. L., On the total geostrophic circulation of the Pacific Ocean: Flow patterns, tracers and transports, *Prog. Oceanogr., 39,* 263-352, 1997.

Rhines, P. B., and W. R. Young, Homogenization of potential vorticity in planetary gyres, *J. Fluid Mech., 122,* 347-367, 1982a.

Rhines, P. B., and W. R. Young, A theory of wind-driven circulation, I, Mid-ocean gyres, *J. Mar. Res., 40,* suppl., 559-596, 1982b.

Robbins, P. E., and J. M. Toole, The dissolved silica budget as a constraint on the meridional overturning circulation of the Indian Ocean, *Deep Sea Res., Part I, 44,* 879-906, 1997.

Stammer, D., Global characteristics of ocean variability estimated from regional TOPEX/POSEIDON large-scale sea surface topography observations, *J. Phys. Oceanogr., 27,* 1743-1769, 1997.

Sverdrup, H. U., M. W. Johnson, and R. H. Fleming, *The Oceans: Their Physics, Chemistry, and General Biology,* 1087 pp., Prentice-Hall, Englewood Cliffs, N.J., 1942.

Talley, L. D., Ventilation of the subtropical North Pacific: The shallow salinity minimum, *J. Phys. Oceanogr., 15,* 1985.

Talley, L. D., Potential vorticity distribution in the North Pacific, *J. Phys. Oceanogr., 18,* 89-106, 1988.

Talley, L. D., Antarctic Intermediate Water in the South Atlantic, in *The South Atlantic: Present and Past Circulation,* edited by G. Wefer, W. H. Berger, G. Siedler, and D. J. Webb, pp. 219-238, Springer-Verlag, New York, 1996.

Talley, L. D., and M. O. Baringer, Preliminary results from WOCE hydrographic sections at 80°E and 32°S in the Central Indian Ocean, *Geophys. Res. Lett., 24,* 2789-2792, 1997.

Talley, L. D., and M. S. McCartney, Distribution and circulation of Labrador Sea Water, *J. Phys. Oceanogr., 12,* 1189-1205, 1982.

Toole, J. M., and B.A. Warren, A hydrographic section across the subtropical South Indian Ocean, *Deep Sea Res., Part I, 40,* 1973-2019, 1993.

Warren, B. A., Transindian hydrographic section at lat. 18°S: Property distributions and circulation in the South Indian Ocean, *Deep Sea Res., Part A, 28,* 759-788, 1981.

Warren, B. A., The deep water of the Central Indian Basin, *J. Mar. Res., 40,* suppl., 823-860, 1982.

You, Y., Dianeutral mixing in the thermocline of the Indian Ocean, *Deep Sea Res., Part I, 43,* 291-320, 1996.

You, Y., Seasonal variations of thermocline circulation and ventilation in the Indian Ocean, *J. Geophys. Res., 102,* 10,391-10,422, 1997.

You, Y., and T. J. McDougall, Neutral surfaces and poten-

tial vorticity in the world's oceans, *J. Geophys. Res., 95,* 13,235-13,261, 1990.

You, Y., and M. Tomczak, Thermocline circulation and ventilation in the Indian Ocean derived from water mass analysis, *Deep Sea Res., 40,* 13-56, 1993.

Young, W. R., and P. B. Rhines, A theory of wind-driven circulation, II, Circulation models and western boundary layer, *J. Mar. Res., 40,* 849-872, 1982.

M. C. McCarthy and L. D. Talley, Scripps Institution of Oceanography, University of California, San Diego, 9500 Gilman Drive, 0230, La Jolla, CA 92093-2030. (e-mail: mcmccarthy@ucsd.edu; ltalley@ucsd.edu)

(Received May 5, 1998; revised October 23, 1998; accepted January 12, 1999.)